https://doi.org/10.5194/egusphere-2026-2508
Preprint. Discussion started: 22 May 2026

Technical note: Guidance on setting up Pecube inversions with the neighbourhood algorithm

Maxime Bernard[1], Georgina E. King[1], Pieter van der Beek[2], Isabel Wapenhans[2], Lingxiao Gong[3], Xavier Robert[4]

[1]Institute of Earth Surface Dynamics, Université de Lausanne, Lausanne, Switzerland.
[2]Institut für Geowissenschaften, Universität Potsdam, Karl-Liebknecht-Straße 24–25, D-14476 Potsdam, Golm, Germany.
[3]Department of Marine, Earth, and Atmospheric Sciences, North Carolina State University, Raleigh, NC, USA.
[4]Institut des Sciences de la Terre (ISTerre), Univ. Grenoble Alpes, Univ. Savoie Mont Blanc, CNRS, IRD, Univ. Gustave Eiffel, Grenoble, France.

Correspondence to: Maxime Bernard (maxime.bernard@unil.ch)

Abstract.

Pecube is a three-dimensional thermal-kinematic model that enables the prediction of thermochronometry data and the investigation of past tectonic and topographic change, using both forward and inverse modelling approaches. However, the problems addressed by Pecube inversions are typically non-linear and high-dimensional, such that multiple models can often reproduce the data equally well. Pecube inversions, which involve the evaluation of large numbers of forward models against observations, are performed using the neighbourhood algorithm (NA), enabling guided exploration of the parameter space. Despite more than a decade of applications, practical guidance on how to configure NA–Pecube inversions remains limited. Furthermore, the recent development of a user-friendly interface for Pecube is expected to broaden its user base and further increase the need for clear guidelines on NA configuration. This contribution aims to provide intuition and general guidance for performing NA–Pecube inversions through a conceptual approach. Although the proposed guidelines remain intentionally broad and do not guarantee optimal performance for user-specific problems, they are intended to support informed decision-making and to provide a practical starting point for NA–Pecube inversions. Users are encouraged to explore and adapt NA tuning parameters to their specific modelling objectives and problem settings.

1 Introduction

Quantifying the timing and rates of landscape modification or rock exhumation in response to tectonic and climatic forcing has been a central focus of research over the past decades (e.g., Montgomery et al., 2001; Whipple, 2009; Champagnac et al., 2012, Adams et al., 2020), and thermochronological dating techniques have proven powerful for such purposes (e.g., Reiners and Brandon, 2006; Berger et al., 2008; Shuster et al. 2011; Glover et al., 2023; Boone et al., 2025). By recording the timing

https://doi.org/10.5194/egusphere-2026-2508
Preprint. Discussion started: 22 May 2026

at which minerals cool below their characteristic closure temperatures, thermochronometers provide constraints on the exhumation of rocks through the upper crust, providing assumptions or independent estimates on the geothermal gradient. Linking measured thermochronometry data to cooling, exhumation, and ultimately the tectonic and/or climatic forces driving this requires modelling the kinematic, topographic and thermal evolution of the crustal region studied. Pecube (Braun, 2003; Braun et al., 2012) is a widely used software package for predicting thermochronometry data arising from 3D simulations of coupled landscape evolution and tectonic scenarios. A forward-modelling approach, in which a model is used to generate synthetic data, can be employed to compare these predictions with observed thermochronometry data. Although useful, such an approach is generally restricted to testing a limited number of working hypotheses, for example regarding topographic evolution (e.g., Whipp et al., 2009; Capaldi et al., 2022) or styles of tectonic exhumation (e.g., Whipp et al., 2007; Robert et al., 2009; McQuarrie and Ehlers, 2017; Thiede et al., 2017) and does not allow a comprehensive exploration of the full range of parameter values that control rock exhumation. For this purpose, inversion approaches are preferred, in which large ensembles of candidate models are systematically evaluated by comparing observations and predictions using an objective (misfit) function (e.g., Ketcham, 2005; Fox and Carter, 2020).

In geosciences, inversion problems are often non-linear, non-unique and high-dimensional, and the number of models that can be evaluated is constrained by computational cost. Consequently, several inversion strategies have been developed to guide exploration of the parameter space toward regions of low misfit and thereby increase inversion efficiency. Broadly, both local and global approaches have been investigated. Local approaches exploit the local curvature of the misfit landscape and iteratively update a model from an initial guess to minimize this function. Examples include steepest descent (e.g., Schuster, 2017), conjugate gradient (e.g., Kelber et al., 2008) and Gauss–Newton methods (e.g., Pratt et al., 1998). These methods can be efficient in locating a nearby minimum but may be less effective for problems with multiple local minima, expensive forward-model evaluations, or when no good initial guess is available.

Global stochastic search (or direct search) methods are designed to explore parameter spaces more broadly by employing probabilistic sampling strategies. In this way, they are more likely to identify multiple acceptable solutions, although they are often less efficient than local deterministic approaches in terms of convergence speed. Examples of global methods include Monte Carlo sampling, in which exploration is purely random (Hammersley and Handscomb, 1964) but which is generally inefficient in such cases, particularly for high-dimensional problems. More advanced methods include: simulated annealing (SA), where exploration is controlled by a temperature parameter that affects how broad the next sampling of the parameter space is and gradually decreases with the misfit (Rothman, 1985); genetic algorithms that use populations of models, crossover and mutation techniques to explore the parameter space (GA; Holland, 1975; Gallagher and Sambridge, 1994); and the Neighbourhood Algorithm (NA; Sambridge, 1999a). The NA is a global, geometry-based direct search method that adaptively samples parameter space using a Voronoi tessellation (Voronoi, 1908). New models are drawn preferentially from regions associated with lower misfit, while still allowing exploration of less-sampled areas, thereby balancing exploitation and exploration. A subsequent appraisal stage enables Bayesian estimation of parameter uncertainties and trade-offs using the ensemble of sampled models (Sambridge, 1999b).

https://doi.org/10.5194/egusphere-2026-2508
Preprint. Discussion started: 22 May 2026

Because of its relatively high computational cost and the non-linearity of the underlying thermal-kinematic problems, Pecube inversions use the Neighbourhood Algorithm (NA; Sambridge et al., 1999) to search for well-fitting regions of parameter space. While Pecube inversions using NA have been applied for more than a decade (e.g., Braun and Robert, 2005; Herman et al., 2007, 2010; Glotzbach et al., 2011; Robert et al., 2011; Coutand et al., 2014; Curry et al., 2021; Wolff et al., 2021; Fan et al., 2022; Gong et al., 2026) and the fundamentals of NA have been presented in Sambridge et al. (1999a), building intuition on how to best configure NA–Pecube inversions in order to achieve both reliable exploration of parameter space and robust inferences remains a recurrent challenge for new Pecube users. While broad guidance on setting up NA has been provided in previous studies (e.g., Braun et al., 2012; Glotzbach et al., 2011; Valla et al., 2010), no contribution yet focused on how to set up NA for Pecube inversions. The recent development of a user-friendly interface for Pecube (Bernard et al., submitted to GChron) is expected to broaden its user base, particularly by attracting new and less experienced users, providing additional motivation for further guidance on NA-Pecube inversions.

This contribution aims to provide a general intuitive picture on the core functionality of NA and its concepts for Pecube users as well as some broad guidance on setting up NA-Pecube inversions. It is stressed that this guidance by no means guarantees appropriate use of NA for a user-specific problem but rather must be seen as a starting point for performing NA-Pecube inversions. Since optimal inversion schemes strongly depend on the exact scenario being tested, as well as the data available, Pecube users are encouraged to test NA tuning parameter combinations on their own.

2 Pecube and the Neighbourhood Algorithm

2.1. Inverse modelling with Pecube

A short description of Pecube is provided here; a full description of its foundations is available in Braun et al. (2003, 2012). Pecube is a three-dimensional thermal-kinematic model that solves the heat-transport equation and predicts thermochronometry data from prescribed topographic and tectonic evolution scenarios. Boundary conditions consist of a constant basal temperature and a time-varying surface temperature controlled by evolving topography. The kinematic formulation allows for spatially and temporally variable vertical and lateral rock advection, either as coherent tectonic blocs or along faults. Compared to thermochronological modelling tools such as QTQt (Gallagher et al., 2012) and HeFTy (Ketcham, 2005), Pecube enables the evaluation of spatially distributed thermochronometry datasets within defined tectonic-geomorphic scenarios. This capability allows direct interpretation of model results in terms of past tectonic or climatic forcing (e.g., Glotzbach et al., 2011; Gong et al., 2026) as well as the design of targeted sampling strategies (e.g., Valla et al., 2011). But this advanced parameterisation introduces a large number of unknown parameters, often limiting the range of scenarios that can be tested. In practice, the complexity of both the datasets and the plausible tectonic-geomorphic histories typically require an inverse modelling approach, in which large numbers of models are evaluated using an objective (misfit) function.

https://doi.org/10.5194/egusphere-2026-2508
Preprint. Discussion started: 22 May 2026

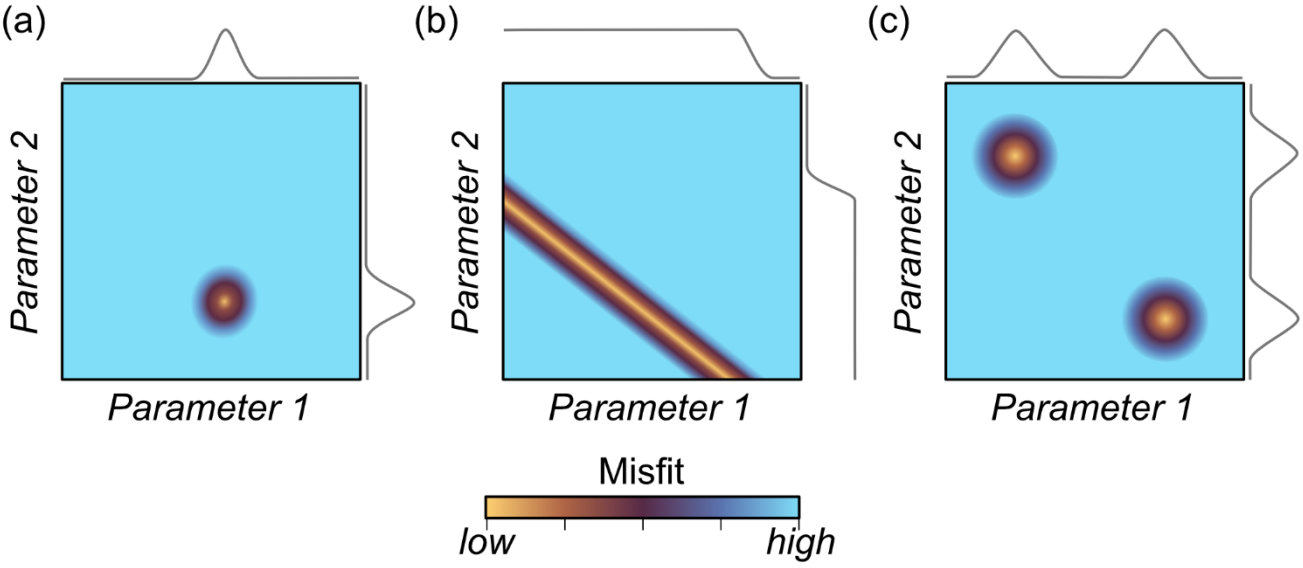

Figure 1. Conceptual misfit landscapes with different complexities. Consider a two-dimensional problem defined by two parameters. A misfit landscape arising from a well constrained problem (a) would show a well-defined area of solutions with low misfit values (orange area) and unimodal posterior probability distribution (PPD, single peaks represent high probability for each parameter value). However, two parameters can show trade-off and provide a range of solutions despite precise data (orange area, b), leading to broad range in the PPDs (no clear peaks for each parameter, b). Additional complexity arises when the misfit landscape incorporates multiple and distinct solutions (local basins, c) leading to multimodal PPDs (here two peaks of high probability for each parameter).

Prior to defining guidelines for the use of the NA, it is necessary to clarify the objectives of Pecube inverse modelling. Inverse approaches allow systematic exploration of a parameter space, defined by prior estimates of the plausible range of parameter values, reflecting research questions such as the timing of topographic change or fault activity, or more generally temporal variations in rock exhumation rates. The combination of data constraints, parameter dimensionality, and prior ranges defines a misfit landscape, the structure of which reflects the range of "acceptable" solutions (i.e., parameter combinations that lead to scenarios fitting the data according to a prescribed objective function). Owing to data limitations (precision and quantity), observational uncertainties (data and models), and parameter trade-offs, even a well-posed problem is expected to admit multiple solutions consistent with the observations.

Consider a hypothetical two-dimensional problem. The misfit landscape may be characterized by a single, well-defined low-misfit basin and unimodal posterior probability distributions (Fig. 1a). More complex cases may exhibit parameter trade-offs, leading to broad posterior distributions (Fig. 1b), or multiple distinct low-misfit regions, resulting in multimodal solutions (Fig. 1c). Consequently, one objective of a Pecube inversion would be to characterize the range and structure of acceptable solutions rather than to identify a single best-fitting model. Although exhaustive random sampling would, in

https://doi.org/10.5194/egusphere-2026-2508
Preprint. Discussion started: 22 May 2026

principle, achieve this goal, limited computational resources constrain Pecube inversions. Effective inversion strategies must therefore balance comprehensive exploration of parameter space with computational efficiency.

2.2. NA-Pecube inversion

2.2.1. Description of the neighbourhood algorithm

The NA comprises two distinct stages: a sampling stage, which guides the exploration of the parameter space, and an appraisal stage, which is used to infer Bayesian descriptors of model resolution, typically framed as posterior probability distributions (PPDs) of the inverted parameters. The sampling stage is coupled to Pecube, whereas the appraisal stage is currently implemented in an external program (NA-Bayes; Sambridge, 2013a). Comprehensive methodological descriptions of both stages are provided in Sambridge (1999a, 1999b) and readers are encouraged to refer to these studies. This contribution focuses exclusively on the sampling stage and presents a concise overview of the underlying philosophy of the NA.

The NA is both a sampler and an optimisation algorithm, in that the exploration of parameter space is adaptively directed towards regions that exhibit favourable data fits. The sampling stage employs a direct-search strategy to minimise the misfit function within a multidimensional (N_d) parameter space. A key principle of NA is the use of information from previously evaluated models to construct a local approximation of the misfit landscape, which is then used to guide subsequent sampling towards regions associated with lower misfit values (i.e., misfit basins; Sambridge, 1999a). The algorithm proceeds iteratively, with each iteration consisting of a batch of forward-model evaluations, the results of which progressively refine the approximation of the misfit landscape (Fig. 2).

Four user-defined parameters control the performance (efficiency and behaviour) of the sampling stage (Table 1): (i) the number of models sampled in the first iteration (N_m^{1st}), (ii) the number of models generated per iteration (N_m), (iii) the number of Voronoi cells (i.e., regions of the parameter space) to resample at each iteration (N_r), and (iv) the number of iterations (N_{it}). The sampling stage of the NA can be summarised in three main steps (Fig. 2). First, an initial ensemble of N_m^{1st} forward models is generated, with model parameters drawn randomly from uniform distributions within their prescribed bounds. This initial

Table 1. Description of NA tuning parameters.

Parameter	Description
N_m^{1st}	Number of models in the first NA iteration
N_r	Number of Voronoi cells to resample at each iteration (best regions)
N_m	Number of models at each iteration
N_{it}	Number of iterations
N_m / N_r	Number of models per Voronoi cell
N_r / N_m	Exploration/exploitation ratio

https://doi.org/10.5194/egusphere-2026-2508
Preprint. Discussion started: 22 May 2026

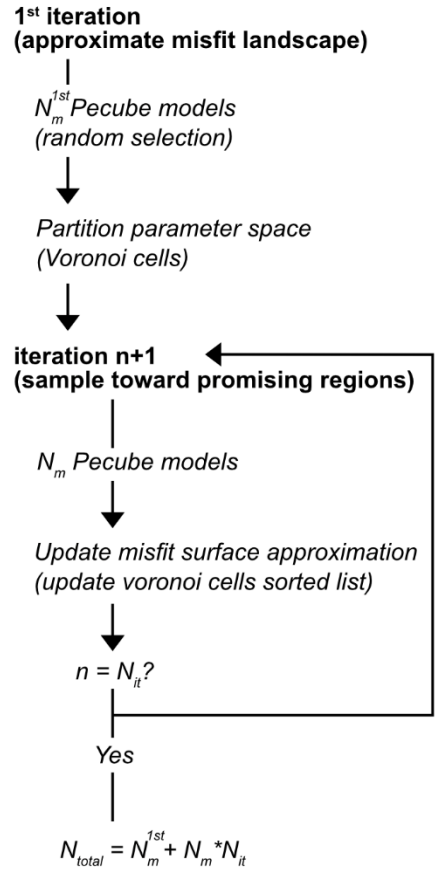

Figure 2. Pecube model generation during an inversion with the neighbourhood algorithm.

iteration is treated separately from subsequent iterations and serves to provide an unbiased first-order exploration of parameter space, allowing a preliminary approximation of the misfit landscape prior to targeted sampling.

Following misfit evaluation, the initial ensemble of sampled models is used to partition the parameter space into Voronoi cells. Before each subsequent iteration, models are ranked according to their relative misfit, rather than their absolute misfit values. This ranking strategy renders the search independent of the magnitude of data errors and of assumptions regarding their statistical distribution (Sambridge, 1999a). The Voronoi cells associated with the N_r best-ranked models are then selected for resampling. A new ensemble of N_m models is generated by sampling within the selected N_r Voronoi cells (Fig. 2). Each selected cell is sampled at least once, requiring that $N_m \geq N_r$. The ratio N_m/N_r controls the number of samples drawn per cell. When this ratio is an integer, all selected cells are sampled equally; otherwise, additional samples are preferentially allocated to the lowest-misfit cells according to the ranking order. The distribution of the newly generated models is then used to update the global Voronoi tessellation, and the algorithm proceeds to the next iteration until the prescribed number of iterations, N_{it}, is reached (Fig. 2).

The total number of forward models performed during each Pecube inversion is therefore:

$$N_{total} = N_m^{1st} + N_m * N_{it}. \quad (1)$$

2.2.2. Role of NA tuning parameters

The ability of the NA to efficiently locate low-misfit regions is controlled by the parameters N_m and N_r, which together regulate the balance between exploration (searching widely across parameter space) and exploitation (focusing on favourable regions). To illustrate these effects, a 2-D parameter space example is considered with a hypothetical misfit landscape incorporating two distinct basins (Fig. 3). Two NA iterations are shown with different N_r/N_m ratios but the same total number of models (N_{total} = 20, Fig. 3). Ten models are randomly sampled in the first iteration (N_m^{1st} = 10), and the parameter space is divided into ten Voronoi cells.

The first case illustrates a strategy dominated by exploitation of the parameter space (Fig. 3a). When all N_m models are drawn exclusively from the single best-ranked Voronoi cell (e.g., $N_r/N_m = 0.1$), sampling rapidly concentrates within a local

https://doi.org/10.5194/egusphere-2026-2508
Preprint. Discussion started: 22 May 2026

low-misfit region. Although this approach accelerates convergence, it substantially increases the likelihood of missing other acceptable solutions; in this example, the low-misfit basin located in the lower left of the parameter space is not sampled (Fig. 3a).

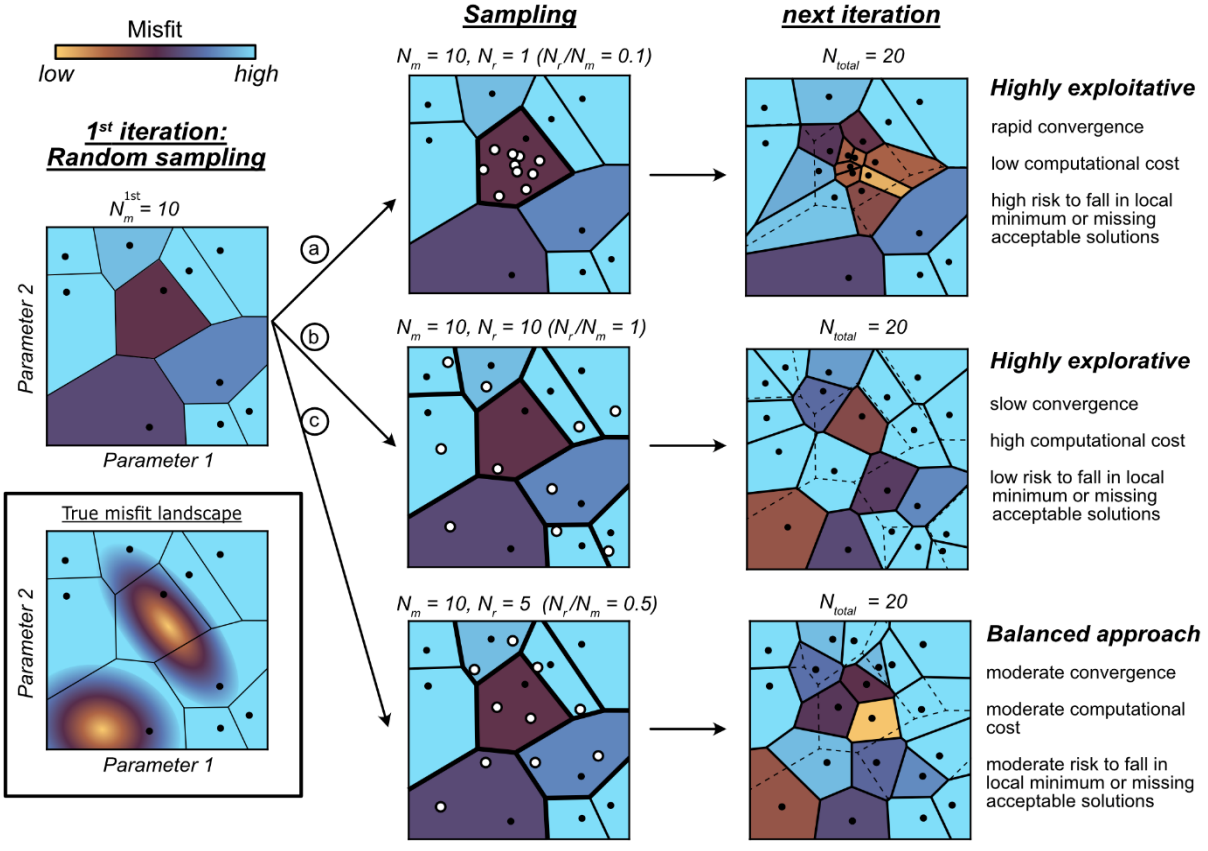

Figure 3. Schematic example of the sampling stage of the Neighbourhood Algorithm (NA). The role of parameters N_m and N_r in controlling the exploration of the parameter space is illustrated. The true misfit landscape of a problem with two misfit minima (or basins) is shown in the inset square. NA samples the parameter space at each iteration and updates the estimated misfit landscape. In the first iteration, NA samples $N_m^{1st} = 10$ models in the two-dimensional parameter space, misfits are evaluated and the parameter space is partitioned into Voronoi cells. In the next iteration, NA is set to sample (a) 10 models in the best fit Voronoi cell ($N_m/N_r = 10$, $N_r/N_m = 0.1$), (b) 10 models in each of the initial Voronoi cells ($N_m/N_r = 1$, $N_r/N_m = 1$), and (c) 10 models in the 5 best Voronoi cells ($N_m/N_r = 2$, $N_r/N_m = 0.5$). The misfits are evaluated for the most recent models and the Voronoi cells are updated. Note how the size of Voronoi cells inversely scales with sampling density.

The second case represents a strategy dominated by exploration (Fig. 3b). Sampling each Voronoi cell once ($N_r/N_m = 1$) ensures broad coverage of parameter space and reduces the risk of convergence towards a spurious local minimum. However, convergence is significantly slower, and a large number of iterations (and thus forward-model evaluations) may be required to adequately characterise the misfit landscape.

https://doi.org/10.5194/egusphere-2026-2508
Preprint. Discussion started: 22 May 2026

The third case illustrates a more balanced strategy (Fig. 3c). Resampling only a subset of the best-ranked Voronoi cells (e.g., $N_r/N_m = 0.5$), with a moderate number of models generated within each cell (in this case, $N_m/N_r = 2$), achieves a compromise between exploration and exploitation. This approach maintains global search capability while progressively focusing sampling towards low-misfit regions, thereby limiting the risk of convergence to suboptimal solutions, such as entrapment within local misfit basins.

In all three cases, the total number of evaluated models is identical (N_{total} = 20, eq. 1), but the resulting approximations of the misfit landscape differ markedly, with strategies dominated by exploration or balanced sampling (cases b and c, Fig. 3) providing a more robust and reliable characterisation of acceptable solutions.

2.2.3. Conceptual tuning of NA parameters

Conceptually, the tuning of NA parameters can be represented by the schematic relationship shown in Figure 4a, which relates the degree of exploration controlled by the ratio N_r/N_m to the number of models generated during the initial iteration (N_m^{1st}). The first iteration corresponds to purely random and unbiased sampling of the parameter space and provides an initial approximation of the misfit landscape. As N_m^{1st} increases, the need for subsequent optimisation decreases, and the appropriate N_r/N_m ratio is therefore expected to decrease accordingly. In case of unlimited computational resources, the misfit landscape could be exhaustively sampled, rendering an optimisation algorithm unnecessary and causing N_r/N_m to tend towards zero. In practice, Pecube inversions are limited to approximately 10^4–10^5 forward models, owing to model dimensionality, which imposes an upper bound on N_m^{1st}.

Conversely, a lower bound on N_m^{1st} is required to ensure a sufficiently representative initial sampling of parameter space, from which meaningful values of N_r can be defined, given that $N_r \leq N_m^{1st}$ (Fig. 4a). Previous studies suggest that N_r/N_m values between 0.5 and 1 are appropriate (Braun et al., 2012; Glotzbach et al., 2011; Valla et al., 2010), as they favour broad exploration of parameter space while limiting the number of samples per Voronoi cell to a maximum of two ($N_m/N_r = 2$). This constraint defines an upper bound for N_r/N_m, which cannot exceed unity (Fig. 4a).

The intersection of these conceptual limits defines a target region in parameter space, within which NA tuning parameters are expected to achieve an effective balance between comprehensive exploration and computational efficiency. Although the precise extent and shape of this target region, as well as the functional relationship between N_r/N_m and N_m^{1st}, remain problem-dependent and are only represented schematically in Figure 4a, this conceptual framework provides practical

https://doi.org/10.5194/egusphere-2026-2508
Preprint. Discussion started: 22 May 2026

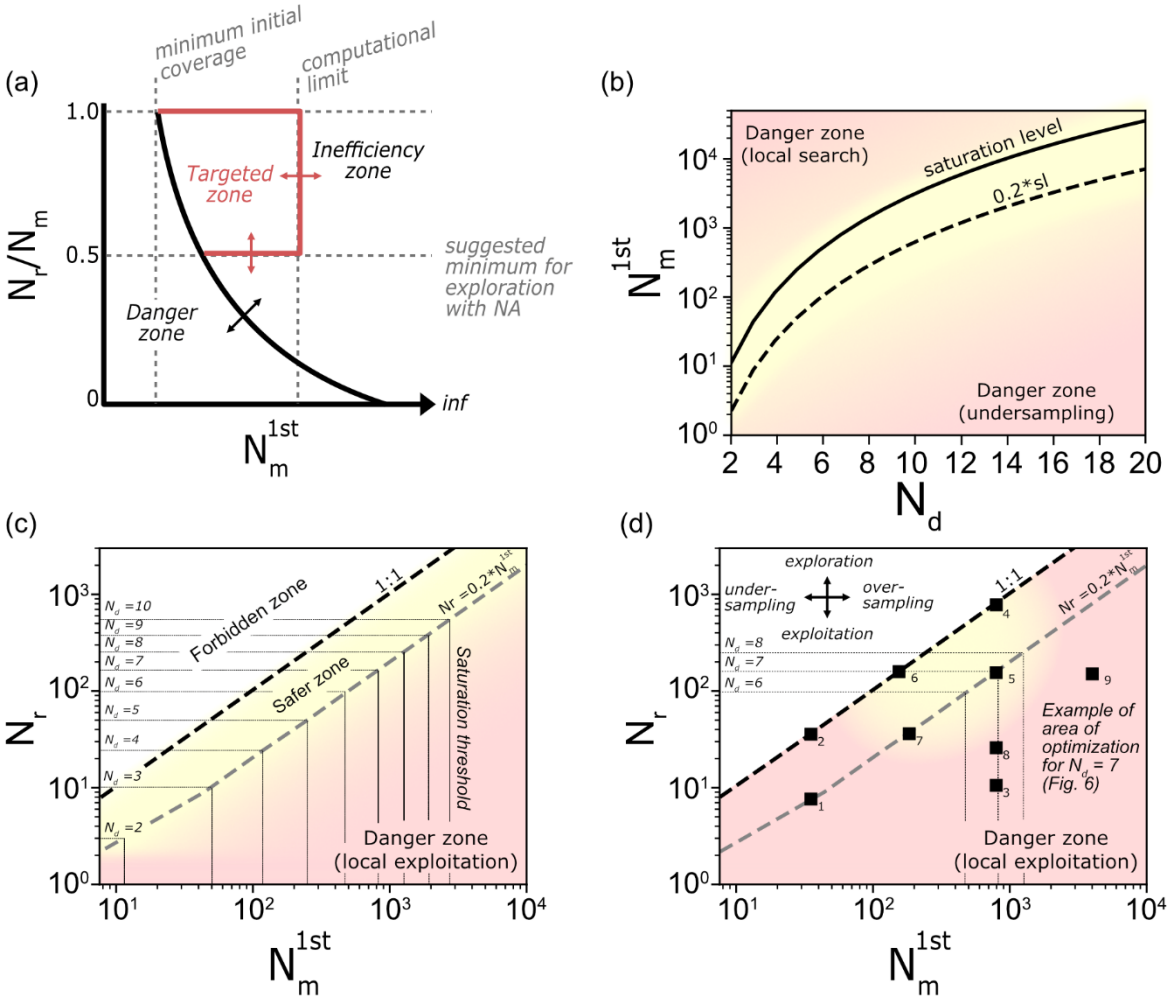

Figure 4. Conceptual exploration of parameter space and guidance in tuning NA parameters. (a) Conceptual diagram showing a hypothetical target zone of NA parameter combinations to consider. (b) Suggested scaling relationship between the number of models to perform in the first iteration of NA and the number of dimension (N_d). (c) Suggested scaling of N_r with N_m^{1st} and dimension. The scaling relationship in (b) is shown as dashed lines for each number of dimension (N_d). (d) Area of NA tuning parameter combinations considered to lead to fair estimation of the misfit landscape for the synthetic example problem in Section 3.1. Squares labelled 1-9 correspond to different combinations of tuning parameters tested in Fig. 7.

guidance for tuning NA parameters in Pecube inversions.

Prescribing universally optimal combinations of NA tuning parameters that would guarantee finding the range of acceptable solutions is out of reach, as these depend on the specific inverse problem. But dropping the objective of finding the most optimal NA parameter combination allows delineation of broad regions of parameter space associated with a higher risk of

https://doi.org/10.5194/egusphere-2026-2508
Preprint. Discussion started: 22 May 2026

failure, particularly the risk of missing acceptable solutions while guiding the selection of more robust configurations. In all cases, users are encouraged to explore the NA parameter combinations that would be appropriate for their specific problem.

Guidance for tuning the number of models in the first iteration (N_m^{1st}) can be drawn from the theoretical analysis of Voronoi tessellations conducted by Sambridge (1998, 2001). These studies investigated how Voronoi geometry evolves with dimensionality, defined here as the number of inverted parameters. They showed that, as the total number of sampled models increases, the average number of neighbours per Voronoi cell asymptotically approaches a threshold, referred to as saturation. Beyond this threshold, Voronoi cells become progressively isolated and lose global connectivity, causing resampling to become increasingly localised in parameter space. Below saturation, resampling of favourable cells retains the ability to reach distant regions of the parameter space, thereby promoting global exploration.

This behaviour is closely linked to the way models are ranked. Consider the true misfit landscape with two local basins illustrated in Fig. 3 and a large number of models generated during the first iteration. When many models exhibit similar misfit values, they are indistinguishable on the basis of rank alone, and the ranking provides no information on their spatial separation in parameter space. As N_m^{1st} approaches saturation, the number of good models within a given basin increase, and many of these models cluster near the top of the ranking list. If N_r is small relative to N_m^{1st}, the selected Voronoi cells may all originate from the same basin, while other basins are excluded from the refinement set. In this case, the neighbourhood algorithm loses its ability to transition between distinct regions of parameter space. This behaviour is less problematic when the primary objective is to characterise the overall misfit landscape but can become preponderant when searching for optimization.

According to Sambridge (2001), the number of models (N) required to reach saturation scales non-linearly with dimensionality according to

$$N \approx N_d^{3.5}. \quad (2)$$

Although this relationship was not explicitly formulated to determine N_m^{1st}, it provides a useful conceptual guide for its tuning. In practice, N may be regarded as an upper reference level for N_m^{1st}. The lower bound of N_m^{1st} is more difficult to define, but at first order it is expected to follow a similar scaling with dimensionality, subject to a minimum requirement of adequately approximating the misfit landscape through initial sampling. In Figure 4b, a lower bound of approximately 0.2N is illustrated for guidance, although this threshold should not be interpreted as a strict constraint. This reasoning provides a practical range of plausible values for N_m^{1st} as a function of problem dimensionality and supports informed tuning of NA parameters.

Following up, how should N_r be tuned? Reasoning similarly as for N_m^{1st}, N_r must be smaller than or equal to N_m^{1st}, as it is not possible to resample more regions of the parameter space than those generated during the first iteration (Fig. 4c). Defining a lower bound for N_r is less straightforward, but taking the reasoning on the saturation expressed above, as N_m^{1st} approaches saturation, the ratio N_r/N_m^{1st} should be adjusted to favour exploration over exploitation. Sampling only a few regions, or only the best-fit regions, would lead to rapid convergence toward a minimum that is likely local and is therefore discouraged (Fig. 3a). As the dimensionality of the problem increases, the misfit landscape becomes more complex, and N_r should therefore increase accordingly. A simple and practical approach is to scale N_r with N_m^{1st}. A lower bound of $N_{r,\text{lower}} = 0.2\,N_m^{1st}$ is

https://doi.org/10.5194/egusphere-2026-2508
Preprint. Discussion started: 22 May 2026

illustrated for guidance. This value is arbitrary and does not guarantee that all acceptable solutions are identified. It should rather be interpreted such that values well above this threshold may lead to satisfactory exploration of the parameter space, whereas values close to or below it increases the risk of missing solutions. The "danger" and "safer" zones shown in Fig. 4b-d should be interpreted as indicative regions of lower or higher confidence rather than strict limits, and their extent depends on the number of dimensions (Fig. 4c-d; Section 3). Specifically, the "safer" zone can be considered a conservative approach that trades optimisation for robustness.

How about N_m? N_m should be chosen to favour exploration by remaining within the range $N_r \leq N_m \leq 2N_r$, corresponding to $0.5 \leq N_r/N_m \leq 1$. Increasing N_m beyond this range increases the number of models evaluated within each Voronoi cell and shifts the balance toward exploitation. For values of N_m significantly larger than $2N_r$, exploration is reduced and the probability of missing acceptable solutions increases.

Lastly, rather than focusing on the number of iterations, the total number of models performed is a more relevant measure when considering the effect of dimensionality. Based on Eq. (2), satisfying coverage of parameter space can generally be expected for $10N \leq N_{total} \leq 50N$. Users can evaluate the convergence of NA by looking at the evolution of the misfit values over iterations. If the range of misfit values per iteration do not vary significantly, convergence can be considered to have been achieved. The following section evaluates these concepts using a synthetic example.

3 Testing the performance of the NA-Pecube inversion

Evaluation of Pecube model predictions with observed data is achieved through an objective (misfit) function. NA can accommodate a wide range of objective functions, but Pecube inversions commonly employ the reduced chi-squared statistic (Braun and Robert, 2005; Braun et al., 2012):

$$\Phi = \frac{1}{\nu}\sum_{j=1}^{N_T}\sum_{i=1}^{N_{o,j}}\left(\frac{A_{i,j}^{obs} - A_{i,j}^{pred}}{\sigma_{i,j}}\right)^2, \quad (3)$$

where N_T is the number of thermochronometers, $N_{o,j}$ is the number of observations (i.e., ages) for the j-th thermochronometer, $A_{i,j}^{obs}$ and $A_{i,j}^{pred}$ are the observed and predicted ages, respectively, and $\sigma_{i,j}$ is the uncertainty associated with $A_{i,j}^{obs}$. The degree of freedom $\nu = N - N_d - 1$ normalises the misfit, where N is the total number of observations, and N_d the number of inverted parameters (i.e., the dimensionality of the parameter space). Note that this approach is only meaningful when $N - N_d > 1$; in practice we would advise $N >> N_d$. Using the reduced chi-squared statistic and the synthetic case allows us to estimate the range of acceptable solutions corresponding to models with $\Phi < 4$ (within 2 sigma data uncertainty on average).

https://doi.org/10.5194/egusphere-2026-2508
Preprint. Discussion started: 22 May 2026

3.1. The exhumation model

To evaluate the concepts outlined above, a synthetic exhumation model is designed using Pecube to generate thermochronometer ages that are subsequently compared with model predictions through a misfit function (Eq. 3) during NA–Pecube inversions. The model considers the real topography of the Mont-Blanc massif in the Western European Alps, covering an area of approximately 40 × 30 km (Fig. 5a). Following the findings of Glotzbach et al. (2011), the imposed exhumation history comprises two stages of tectonic uplift combined with two stages of topographic evolution. The tectonic scenario initiates at 20 Ma with a rock uplift rate of $U_1 = 0.9$ km Myr^{-1} until 6.5 Ma (Fig. 5c), after which the uplift rate decreases to $U_2 = 0.3$ km Myr^{-1}. Simultaneously, the topography evolves from an initial plateau at approximately 4 km elevation and undergoes continuous incision until $t_R = 1$ Ma, reaching half of the present-day relief ($R = 0.5$, Fig. 5c). This scenario results in enhanced valley incision rates during the last 1 Myr, consistent with the scenario proposed by Glotzbach et al. (2011). Other parameters include the model thickness set to 30 km, the thermal diffusivity ($\kappa = 30$ km² Myr^{-1}), the basal temperature ($T_b = 600$ °C), the heat production rate ($H_p = 14$ °C Myr^{-1}), the temperature at sea-level ($T_{sl} = 12.5$ °C) and the atmospheric lapse rate ($\beta = 6$ °C km^{-1}).

Based on the prescribed exhumation history and the associated rock cooling paths, a synthetic dataset comprising 51 thermochronometry ages is generated (Fig. 5b-5d). The dataset includes three thermochronometers, apatite (U–Th)/He (AHe), apatite fission-track (AFT), and zircon fission-track (ZFT) from 17 surface samples (Fig. 5b), thereby representing a well-defined sampling strategy following Valla et al. (2011). Thermochronometer ages are predicted using the kinetic models of Farley et al. (2000), Ketcham et al., (2007) and Rahn et al. (2004) for AHe, AFT and ZFT, respectively. To move away from perfectly predicted data, each age is assigned a random noise within 10 % its original value (Fig. 5d). For the subsequent inversions, all synthetic ages are assigned a uniform uncertainty of 5 %, corresponding to relatively precise data.

https://doi.org/10.5194/egusphere-2026-2508
Preprint. Discussion started: 22 May 2026

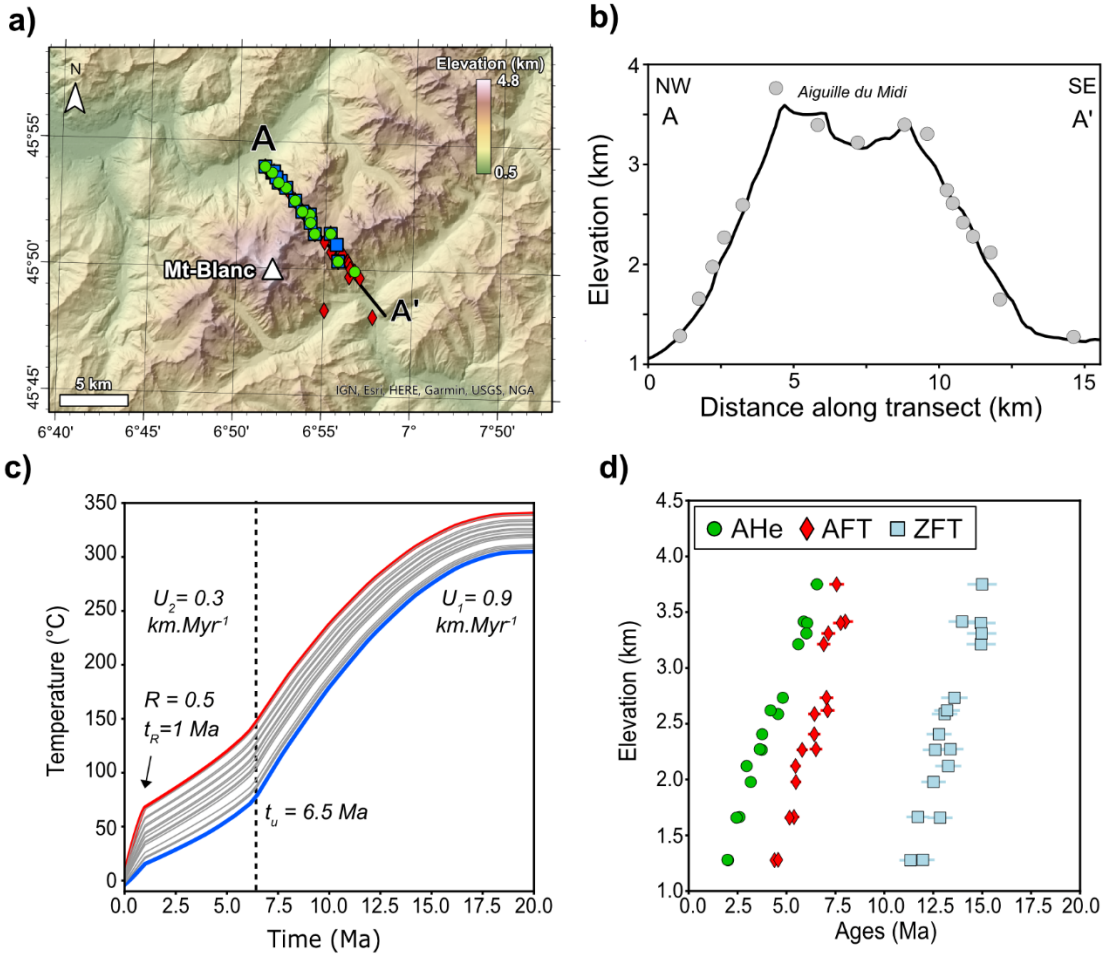

Figure 5. Synthetic exhumation and cooling history prescribed in Pecube to generate data. The rock exhumation comprises two stages with rock uplift rates U_1 = 0.9 km Myr^{-1} and U_2 = 0.3 km Myr^{-1}, with a time of change between stages t_u = 6.5 Ma. Simultaneously, topographic incision occurs from a 4-km-high initial plateau at 20 Ma, incising to half the present-day relief at t_R = 1 Ma, and enhanced valley incision rates during the last 1 Myr. (a) Model extent of the Mont-Blanc area with synthetic samples outlined (DEM from NASA Shuttle Radar Topography Mission; SRTM, 2013). (b) Topographic profile along the sample transects (profile A-A' in a). (c) Resulting rock cooling path for all samples, the coldest and hottest cooling histories are highlighted in blue and red respectively. (d) Thermochronometer age predictions following the cooling histories in c, for apatite (U-Th)/He (AHe), and apatite (AFT) and zircon (ZFT) fission-track with additional random noise within 10 % original predictions and 5 % uncertainty. See main text for discussion.

https://doi.org/10.5194/egusphere-2026-2508
Preprint. Discussion started: 22 May 2026

3.2. NA-Pecube inversions and estimated posterior probability distribution

Different NA tuning strategies and their estimated posterior probability distribution (PPD) are evaluated against the true PPD of the problem (Figs. 6 and 7), the latter having been determined by a thorough (and costly) random exploration of the parameter space. The goal is to assess the accuracy of each inversion in recovering the range of acceptable solutions. The inverse problem involves seven unknown parameters: t_u, U_1, U_2, t_R, R, T_b and H_p (Fig. 5c), corresponding to a seven-dimensional parameter space, while all other parameters described in Section 3.1 are supposed known and fixed to their true values.

Based on the conceptual framework illustrated in Fig. 4c, four end-member combinations of NA tuning parameters are selected for demonstration (inversions 1-4, Fig. 4d) defined by different values of N_m^{1st} and N_r (Fig. 4d). They consider cases of under-sampled/exploitative (inversion 1, Fig. 4d), under-sampled/explorative (inversion 2, Fig. 4d), over-sampled/exploitative (inversion 3, Fig. 4d), and over-sampled/explorative (inversion 4, Fig. 4d) NA configurations. Additional NA configurations (inversions 5-9, Fig. 4d) are also considered to help define the area of fair NA configuration for this synthetic example. For all inversions, the number of models sampled per Voronoi cell is set equal to the number of resampled cells ($N_m = N_r$, i.e., $N_r/N_m = 1$) to maximize exploration. Each inversion evaluates a total of 30000 models, a number that exceeds by far the saturation threshold expected for a seven-dimensional parameter space ($N(N_d = 7) = 907$, eq. 2).

Figure 6 illustrates the distribution of sampled models and their associated misfit values within scatter plots for the first five end-member NA-Pecube inversions. For each NA configuration, both the sampling density of the parameter space and the ability to approximate the true misfit landscape (Fig. 6a-d) can be assessed. Each parameter shows a relatively broad range of acceptable solutions despite low uncertainties on the data (i.e., 5 %), only parameters t_R and U_2 show restricted values below 5 Ma and 0.5 km Myr^{-1} respectively. The wide range of solutions observed for the true misfit landscape arises because of data resolution (uncertainty, density, scattering) but also arises due to the non-unique solution of the problem. Especially, parameters such as T_b and H_p are highly unconstrained by the data (Fig. 6d), giving alternative good solutions (white and green stars, Fig. 6a-d), and alternative PPDs from the true model (note for instance that the true PPD peaks to ~12 Ma for parameter t_u while the true input value is t_u = 6.5 Ma; Fig. 5c). Therefore, it is important to keep in mind that the "true" solution is given by the misfit landscape of the problem and may be non-unique, giving further support to characterize at best the PPDs.

The first inversion, considering resampling only the first N_r = 7 best regions after an initial exploration with $N_m^{1st} = 36$ models (Fig. 4d), exhibits relatively poor sampling of the parameter space (Fig. 6e-h), resulting in marked difference and under-appreciation of the true misfit landscape, as well as estimated parameter PPDs that differ from the true distributions (inv. 1, Fig. 7a-g). Inversion 2 improves the exploration of the parameter space relative to inversion 1 by resampling more Voronoi cells (N_r = 36 and $N_m^{1st} = 36$ models). Although estimates of the range of "acceptable" solutions retrieved has improved relative to the true distribution (Fig. 6i-l), the discrepancy of estimated PPDs to the true PPDs remains unsatisfying (inv. 2, Fig. 7a-g). Inversion 3 increases the number of models in the first iteration but keep N_r relatively low (N_r = 10, $N_m^{1st} = 900$ models). This configuration improves the initial coverage of the parameter space (Fig. 6m-p) due to the unbiased sampling in the first

https://doi.org/10.5194/egusphere-2026-2508
Preprint. Discussion started: 22 May 2026

iteration. However, the highly exploitative setting (with resampling only N_r = 10 best Voronoi cells), focuses exploitation in restricted area of the parameter space, leading to biased PPDs estimates (inv. 3, Fig. 7a-g). Finally, inversion 4 considering large exploration of parameter space (N_r = 900, $N_m^{1st} = 900$ models) enables a fair estimate of the true misfit landscape and PPDs (Fig. 6q-t; inv. 4, Fig. 7h-n). However, the convergence to an optimal solution has not occurred (appreciate misfit values in Fig. 6q-t) and more iterations and models than the 30000 considered here would be needed. A balance between exploration and exploitation while still recovering a good estimate of the true PPDs can be achieved for instance by increasing exploitation from the previous inversion (inversion 4) and resampling only N_r = 180 models corresponding to 20 % of the N_m^{1st} models (inversion 5, Fig. 6u-x, Fig. 7h-n). Alternative NA configurations are tested and their PPDs shown in Fig. 7 (inv. 6-9) and allow delineation of the "safer zone" for this example as shown in Fig. 4d.

To conclude, broader exploration of the parameter space, either by resampling a larger number of Voronoi cells after the first iteration (inversions 4 and 6; Fig. 4d) and/or by increasing the number of models generated during the first iteration (N_m^{1st}; inversions 5 and 7; Fig. 4d) can be considered good inversion strategies. But threshold values for both NA parameters exist below which exploration is limited and the risk to recover biased PPDs estimates increases. While these threshold values are difficult to estimate and likely depends on the problem being solved (i.e., the complexity of the misfit landscape), the characterisation of the "safer" and "danger" zone here provides an appreciation of NA configurations to avoid.

https://doi.org/10.5194/egusphere-2026-2508
Preprint. Discussion started: 22 May 2026

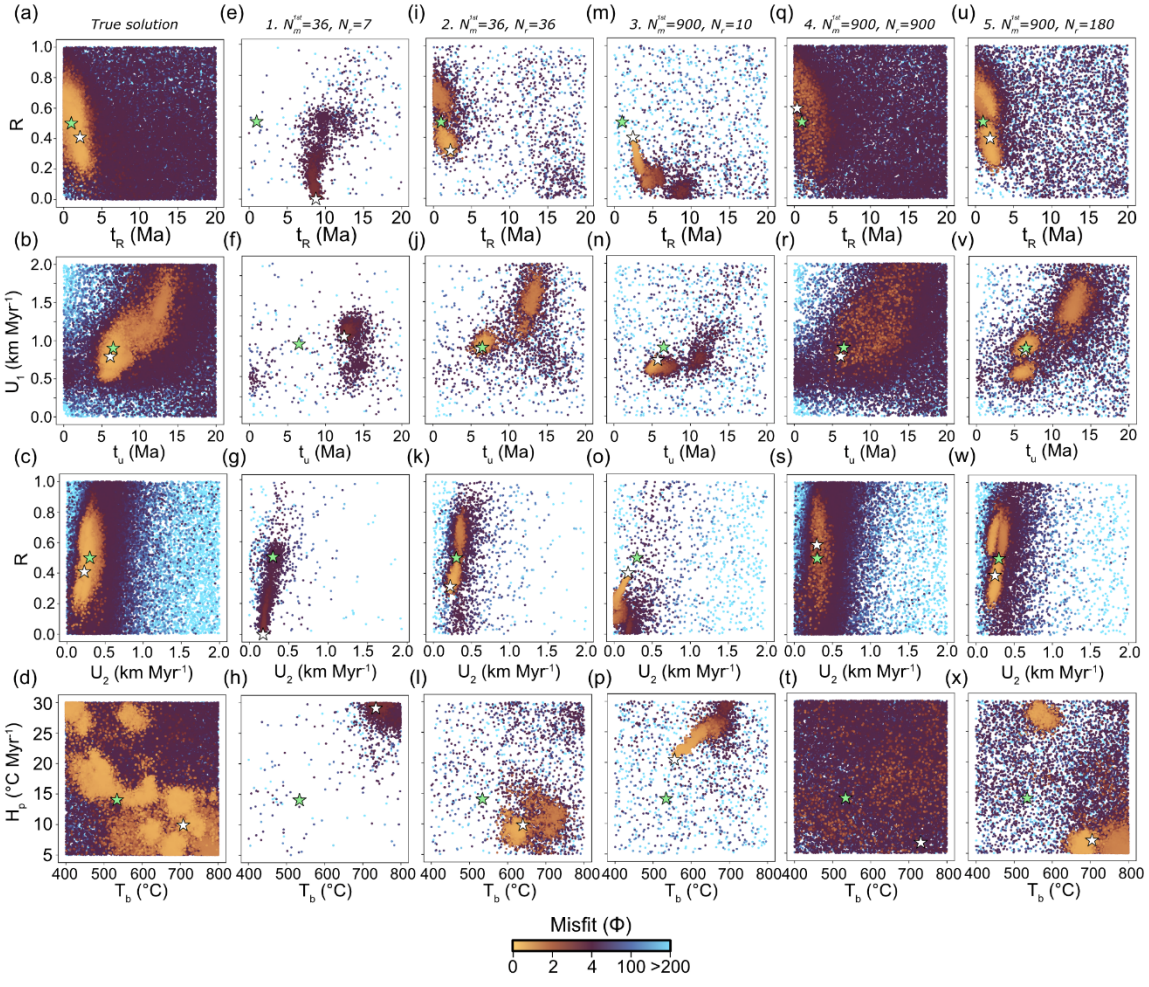

Figure 6. Distribution of sampled models for NA-Pecube inversions considered with the synthetic exhumation scenario. In each plot, white and green stars show the best fit model after each inversion and the true parameter value respectively. (a-d) True misfit distribution inferred from >130000 Pecube forward models. (e-x) Misfit distribution for different combinations of NA tuning parameters ($N_m^{1st}$and N_r; see Fig. 4d). All inversions consider a ratio N_r/N_m = 1 and 30000 forward models evaluated. See text for more details. Scatter plots are generated using the PyPIVoT software (Wapenhans et al., 2025).

4 Summary and conclusion

This contribution presents a conceptual framework intended to guide the configuration of NA–Pecube inversions as a function of problem dimensionality. It forms part of a broader effort to improve the accessibility of Pecube (Bernard et al., submitted to GChron), to clarify the principles underlying the neighbourhood algorithm (Sambridge, 1999a), and to support informed

https://doi.org/10.5194/egusphere-2026-2508
Preprint. Discussion started: 22 May 2026

decision-making when setting up NA–Pecube inversions. It is emphasised that the proposed guidance does not guarantee that all acceptable solutions to a user-specific Pecube problem will be identified; rather, it should be viewed as a first step towards exploring suitable NA configurations.

A summary of the recommended guidelines, together with the rationale underpinning each of them, is provided in Table 2. The discussion is grounded on the premise that Pecube inversions should primarily aim to characterise the structure of the misfit landscape, rather than to identify a single best-fitting model. This rationale follows the philosophy articulated by Sambridge (2013b) that "it is better to get good sampling slowly than poor sampling quickly". For high-dimensional problems, however, slow sampling may become impractical because of computational limitations, and optimisation strategies involving lower N_r/N_m ratios (i.e. <0.5) may be required to achieve convergence towards acceptable solutions. This reflects the exponential increase in the number of models required to adequately sample parameter space as dimensionality increases (Fig. 4b; Eq. 2).

With the concepts illustrated in Figs. 1-4, broad directions for tuning NA-Pecube inversions can be drawn. For relatively precise (i.e, low uncertainty) and dense datasets, the range of acceptable solution is expected to be further confined in specific regions within the misfit landscape and NA should therefore be tuned toward exploration (compass in Fig. 4d). Conversely, relatively imprecise data increase the range of acceptable solutions and broaden regions of low misfit values, requiring less models to achieve a good approximation of the PPD.

These guiding principles can also be extended to favour limiting the range and number of unknown parameters in order to better characterise the range of acceptable solutions, rather than attempting to invert for a large number of poorly constrained parameters and risking the omission of viable solutions. In practice, this implies that the number of inverted parameters in NA–Pecube inversions should be restricted to facilitate exploration and improve understanding of parameter trade-offs. An upper limit of approximately ten parameters can be considered reasonable to enable sufficient exploration, consistent with Eq. 2. Finally, Pecube users are strongly encouraged to explore and test Pecube parameter trade-offs through preliminary experiments before undertaking full NA–Pecube inversions.

https://doi.org/10.5194/egusphere-2026-2508
Preprint. Discussion started: 22 May 2026

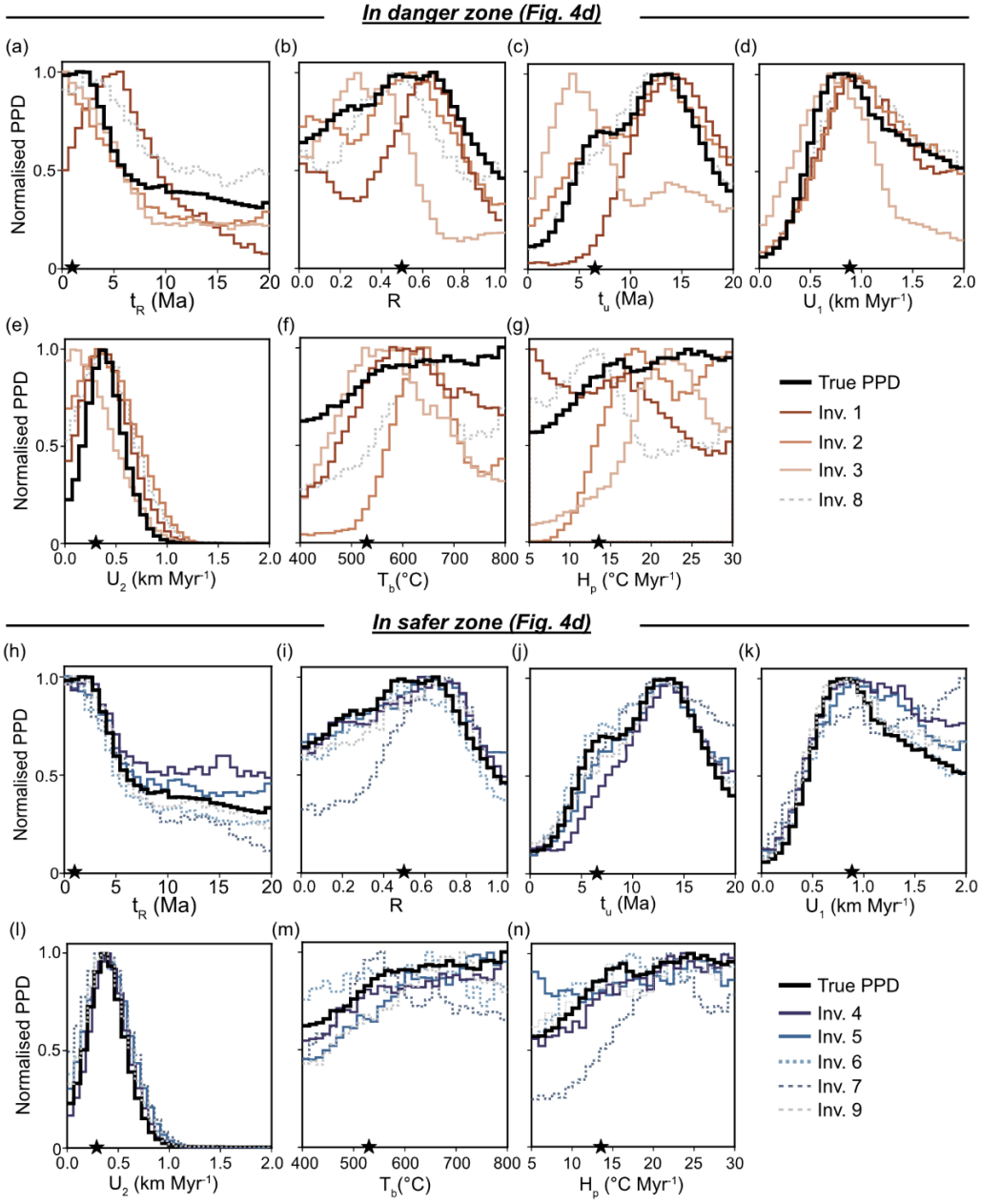

Figure 7. Posterior probability distributions (PPD) for inverted parameter values from the synthetic NA-Pecube inversions. PPDs are shown for the timing of relief change (t_R, a), relief amplification at t_R (R, b), the timing of rock uplift change (t_u, c), the uplift rate during stage 1 (U_1, d), the uplift rate during stage 2 (U_2, e), the basal temperature (T_b, f), and the heat production rate (H_p, g). Black lines correspond to the true PPDs. The plots and PPDs are generated using the neighpy python package (Marignier, 2024).

Table 2. Summary of suggestions for Pecube inversions with NA along with rationales and prevention.

NA parameter/Criterion	Suggested (but not limited to)	Rationale	Discouraged
Number of models in the first iteration (N_m^{1st})	$0.2N_d^{3.5} < N_m^{1st}$ where N_d is the number of dimensions.	❖ A fair first approximation of the misfit landscape is needed to drive NA toward best fit regions. ❖ The number of samples to fill up a parameter space increases non-linearly with dimension.	❖ Too few models that do not allow broad coverage of the parameter space. ❖ Too many models risk NA sampling becoming local (risk of focusing sampling in local basins and missing acceptable other solutions).
Number of Voronoi cells to resample (N_r)	$0.2N_m^{1st} < N_r$	❖ $N_r <= N_m^{1st}$ ❖ Increasing dimension (unknowns) increases the misfit landscape complexity, therefore N_r should scale with dimension and by extent N_m^{1st}.	N_r too small so that exploration is limited to local regions of the parameter space.
Number of models for each subsequent iteration (N_m)	$N_r \leq N_m \leq 2N_r$	NA should be tuned to favour exploration over exploitation to minimize the risk of missing acceptable solutions.	$N_r/N_m < 0.5$ leads to rapid convergence toward (local) minima and can miss acceptable solutions.
Total number of models (N_{total})	$10N_d^{3.5} \leq N_{Total} \leq 50N_d^{3.5}$	The number of samples required to fill up a parameter space increases non-linearly.	$N_{Total} \ll N_d^{3.5}$
Additional suggestions for NA-Pecube inversions			
Number of dimensions (N_d)	Limit N_d to ~10 maximum Use as much a-priori knowledge/assumptions as possible.	❖ To comply with the objective of describing the range of acceptable solutions, NA should be tuned for exploration, and a significant number of models should be performed. ❖ Limiting N_d allows more exploration with given computational resources. ❖ It may be better to describe at best the misfit landscape and better understand trade-off between Pecube parameters, rather than over-optimizing the search algorithm and find a best-fit model but miss valuable information.	Too large number of dimensions so that proper exploration of the parameter space is impossible and convergence to a minimum misfit is relatively insignificant.
NA parameters	Systematically report NA parameters for each inversion (N_m^{1st}, N_r, N_m, N_{total})	❖ Reporting NA parameter values used in NA-Pecube inversion help assessing the robustness of inferences.	Not reporting NA parameter values.

https://doi.org/10.5194/egusphere-2026-2508
Preprint. Discussion started: 22 May 2026

Author contributions. MB designed this study and wrote this manuscript. GEK, PvdB, IW, LG, and XR provided support on the design and writing of the manuscript.

Code and data availability. No data have been used or generated in this manuscript. The Pecube code is available as a github repository: https://github.com/jeanbraun/Pecube/tree/PecubeGUI.

Competing interests. One of the (co-)authors (GEK) is a member of the editorial board of *Geochronology*. No other competing interests to be declared.

Acknowledgements. This work has been funded by the European Research Council (ERC) under the European Union's Horizon 2020 research and innovation programme (Grant agreements No. 851614 to GEK and No. 834271 to PvdB).

References

Adams, B. A., Whipple, K. X., Forte, A. M., Heimsath, A. M., and Hodges, K. V.: Climate controls on erosion in tectonically active landscapes. Science advances, 6(42), eaaz3166, 2020.

Bernard, M., van der Beek, P., Colleps, C., Robert, X., Gallagher, K., Guenthner, W., Amalberti, J., King, G.: PecubeGUI: a user interface for the Pecube thermal-kinematic model and advanced low-temperature thermochronometer predictions, submitted to GChron journal, 21 April 2026.

Berger, A. L., Gulick, S. P. S., Spotila, J. A., Upton, P., Jaeger, J. M., Chapman, J. B., Worthington, L. A., Pavlis, T. L., Ridgway, K. D., Willems, B. A., and McAleer, R. J.: Quaternary tectonic response to intensified glacial erosion in an orogenic wedge, Nature Geoscience, 1, 793–799, https://doi.org/10.1038/ngeo334, 2008.

Boone, S. C., Glorie, S., Zahirovic, S., Nixon, A., Meeuws, F., and Kohlmann, F.: Deciphering mantle, tectonic and climatic drivers of exhumation, Commun. Earth Environ., 6, 1015, https://doi.org/10.1038/s43247-025-03005-6, 2025.

Braun, J.: Pecube: a new finite-element code to solve the 3D heat transport equation including the effects of a time-varying, finite amplitude surface topography, Computers and Geosciences, 29, 787–794, https://doi.org/10.1016/s0098-3004(03)00052-9, 2003.

Braun, J. and Robert, X.: Constraints on the rate of post-orogenic erosional decay from low-temperature thermochronological data: application to the Dabie Shan, China, Earth Surface Processes and Landforms, 30, 1203–1225, https://doi.org/10.1002/esp.1271, 2005.

https://doi.org/10.5194/egusphere-2026-2508
Preprint. Discussion started: 22 May 2026

Braun, J., van der Beek, P., Valla, P., Robert, X., Herman, F., Glotzbach, C., Pedersen, V., Perry, C., Simon-Labric, T., and Prigent, C.: Quantifying rates of landscape evolution and tectonic processes by thermochronology and numerical modeling of crustal heat transport using PECUBE, Tectonophysics, 524–525, 1–28, https://doi.org/10.1016/j.tecto.2011.12.035, 2012.

Capaldi, T. N., Odlum, M. L., Curry, M. E., and Stockli, D. F.: Variable thermal histories across the Pyrenees orogen recorded in modern river sand detrital geo-/thermochronology and PECUBE thermokinematic modelling. Basin Research, 34(5), 1781-1806, 2022.

Champagnac, J. D., Molnar, P., Sue, C., and Herman, F.: Tectonics, climate, and mountain topography. Journal of Geophysical Research: Solid Earth, 117(B2), 2012.

Coutand, I., Whipp, D. M., Grujic, D., Bernet, M., Fellin, M. G., Bookhagen, B., Landry, K. R., Ghalley, S. K., and Duncan, C.: Geometry and kinematics of the Main Himalayan Thrust and Neogene crustal exhumation in the Bhutanese Himalaya derived from inversion of multithermochronologic data, Journal of Geophysical Research, 119, 1446–1481, https://doi.org/10.1002/2013jb010891, 2014.

Crank, J., and Nicolson, P.: A practical method for numerical evaluation of solutions of partial differential equations of the heat-conduction type. In Mathematical proceedings of the Cambridge philosophical society (Vol. 43, No. 1, pp. 50-67). Cambridge University Press, 1947.

Curry, M. E., van der Beek, P., Huismans, R. S., Wolf, S. G., Fillon, C., and Muñoz, J.-A.: Spatio-temporal patterns of Pyrenean exhumation revealed by inverse thermo-kinematic modeling of a large thermochronologic data set, Geology, 49, 738–742, https://doi.org/10.1130/g48687.1, 2021.

Fan, S., Murphy, M. A., Whipp, D. M., Saylor, J. E., Copeland, P., Hoxey, A. K., Taylor, M. H., and Stockli, D. F.: Megathrust heterogeneity, crustal accretion, and a topographic embayment in the Western Nepal Himalaya: Insights from the inversion of thermochronological data, Tectonics, 41, e2021TC007071, https://doi.org/10.1029/2021tc007071, 2022.

Farley, K. A.: Helium diffusion from apatite: General behavior as illustrated by Durango fluorapatite. Journal of Geophysical Research: Solid Earth, 105(B2), 2903-2914, 2000.

Fox, M. and Carter, A.: Heated topics in thermochronology and paths towards resolution, Geosciences, 10, 375, https://doi.org/10.3390/geosciences10090375, 2020.

Gallagher, K.: Transdimensional inverse thermal history modeling for quantitative thermochronology. Journal of Geophysical Research: Solid Earth, 117(B2), https://doi.org/10.1029/2011JB008825, 2012.

Glotzbach, C., van der Beek, P. A., and Spiegel, C.: Episodic exhumation and relief growth in the Mont Blanc massif, Western Alps from numerical modelling of thermochronology data. Earth and Planetary Science Letters, 304(3-4), 417-430, 2011

Glover, C. O., McQuarrie, N., Falkowski, S., and Ehlers, T. A.: Assessing drivers of high exhumation magnitudes and young cooling ages in the eastern central Andes, southern Peru (13–18° S). Earth and Planetary Science Letters, 620, 118281, 2023

Gong, L., van der Beek, P., Sobel, E. R., Schildgen, T. F., Mariotti, A., Bernard, M., Glodny J., and Wapenhans, I.: Late-Cenozoic tectonic versus glacial control on the topographic evolution of the Terskey Range, Kyrgyz Tian Shan. Geology, 2026.

https://doi.org/10.5194/egusphere-2026-2508
Preprint. Discussion started: 22 May 2026

Hammersley, J. M., and Handscomb, D. C.: The general nature of Monte Carlo methods. In Monte carlo methods (pp. 1-9). Dordrecht: Springer Netherlands, 1964.

Herman, F., Braun, J., and Dunlap, W. J.: Tectonomorphic scenarios in the Southern Alps of New Zealand, Journal of Geophysical Research, 112, B04201, https://doi.org/10.1029/2004jb003472, 2007.

Herman, F., Copeland, P., Avouac, J.-P., Bollinger, L., Mahéo, G., Fort, P. L., Rai, S., Foster, D., Pêcher, A., Stüwe, K., and Henry, P.: Exhumation, crustal deformation, and thermal structure of the Nepal Himalaya derived from the inversion of thermochronological and thermobarometric data and modeling of the topography, Journal of Geophysical Research, 115, B06407, https://doi.org/10.1029/2008jb006126, 2010.

Kelbert, A., Egbert, G. D., and Schultz, A.: Non-linear conjugate gradient inversion for global EM induction: resolution studies. Geophysical Journal International, 173(2), 365-381, 2008.

Ketcham, R. A.: Forward and inverse modeling of low-temperature thermochronometry data. Reviews in Mineralogy and Geochemistry, 58, 275, https://doi.org/10.2138/rmg.2005.58.11, 2005.

Ketcham, R. A., Carter, A., Donelick, R. A., Barbarand, J., and Hurford, A. J.: Improved modeling of fission-track annealing in apatite. American Mineralogist, 92(5-6), 799-810, 2007.

Marignier, A.: neighpy - a Python implementation of the Neighbourhood Algorithm for the optimisation and appraisal of high-dimensional loss surfaces, https://github.com/auggiemarignier/neighpy, 2024.

McQuarrie, N. and Ehlers, T. A.: Techniques for understanding fold-and-thrust belt kinematics and thermal evolution, in: Linkages and Feedbacks in Orogenic Systems, edited by: Law, R. D., Thigpen, J R, Merschat, A J, and Stowell, H. H., Geological Society of America Special Publications, 213, 25–54, https://doi.org/10.1130/2017.1213(02), 2017.

Montgomery, D. R., Balco, G., and Willett, S. D.: Climate, tectonics, and the morphology of the Andes. Geology, 29(7), 579-582, 2001.

NASA Shuttle Radar Topography Mission (SRTM): Shuttle Radar Topography Mission (SRTM) Global. Distributed by OpenTopography, https://doi.org/10.5069/G9445JDF, 2013.

Pratt, R. G., Shin, C., and Hick, G. J.: Gauss–Newton and full Newton methods in frequency–space seismic waveform inversion. Geophysical journal international, 133(2), 341-362, 1998.

Rahn, M. K., Brandon, M. T., Batt, G. E., and Garver, J. I.: A zero-damage model for fission-track annealing in zircon. American Mineralogist, 89(4), 473-484, 2004.

Reiners, P. W. and Brandon, M. T.: Using thermochronology to understand orogenic erosion, Annual Review of Earth and Planetary Sciences, 34, 419–466, https://doi.org/10.1007/978-3-540-48684-8, 2006.

Robert, X., van der Beek, P., Braun, J., Perry, C., Dubille, M., and Mugnier, J. L.: Assessing Quaternary reactivation of the Main Central thrust zone (central Nepal Himalaya): New thermochronologic data and numerical modeling. Geology, 37(8), 731-734, 2009.

https://doi.org/10.5194/egusphere-2026-2508
Preprint. Discussion started: 22 May 2026

Robert, X., van der Beek, P., Braun, J., Perry, C., and Mugnier, J.-L.: Control of detachment geometry on lateral variations in exhumation rates in the Himalaya: Insights from low-temperature thermochronology and numerical modeling, J. Geophys. Res.: Solid Earth, 116, B05202, https://doi.org/10.1029/2010jb007893, 2011.

Sambridge, M.: Exploring multidimensional landscapes without a map. Inverse problems, 14 (3), 427-440, 1998.

Sambridge, M.: Geophysical inversion with a neighbourhood algorithm—I. Searching a parameter space, Geophysical Journal International, 138, 479–494, https://doi.org/10.1046/j.1365-246x.1999.00876.x, 1999a.

Sambridge, M.: Geophysical inversion with a neighbourhood algorithm—II. Appraising the ensemble. Geophysical Journal International, 138(3), 727-746, https://doi.org/10.1046/j.1365-246x.1999.00900.x, 1999b.

Sambridge, M.: Finding acceptable models in nonlinear inverse problems using a neighbourhood algorithm. Inverse problems, 17 (3), 387-403, 2001.

Sambridge, M.: NA-Bayes documentation, https://www.iearth.edu.au/codes/NA/NA_Bayes.php, last access: 17 April 2026, 2013a.

Sambridge, M.: NA-Bayes documentation,w.iearth.edu.au/codes/NA/NA_sampler.php, last access: 17 April 2026, 2013b.

Schuster, G. T. (2017). Seismic inversion. Society of Exploration Geophysicists.

Shuster, D. L., Cuffey, K. M., Sanders, J. W., and Balco, G.: Thermochronometry reveals headward propagation of erosion in an alpine landscape. Science, 332(6025), 84-88, 2011.

Thiede, R., Robert, X., Stübner, K., Dey, S., and Faruhn, J.: Sustained out-of-sequence shortening along a tectonically active segment of the Main Boundary thrust: The Dhauladhar Range in the northwestern Himalaya. Lithosphere, 9(5), 715-725, 2017.

Valla, P. G., Herman, F., van Der Beek, P. A., and Braun, J.: Inversion of thermochronological age-elevation profiles to extract independent estimates of denudation and relief history—I: Theory and conceptual model. Earth and Planetary Science Letters, 295(3-4), 511-522, 2010.

Valla, P. G., van der Beek, P. A., and Braun, J.: Rethinking low-temperature thermochronology data sampling strategies for quantification of denudation and relief histories: A case study in the French western Alps. Earth and Planetary Science Letters, 307(3-4), 309-322, 2011.

Voronoi, G.: Nouvelles applications des paramètres continus à la théorie des formes quadratiques. Premier mémoire. Sur quelques propriétés des formes quadratiques positives parfaites. Journal für die reine und angewandte Mathematik (Crelles Journal), 1908(133), 97-102, 1908.

Wapenhans, I., Gong, L., and van der Beek, P.: PyPIVoT (PecubeGUI Visualization Tools). Zenodo. https://doi.org/10.5281/ZENODO.17079595, 2025.

Whipp Jr, D. M., Ehlers, T. A., Blythe, A. E., Huntington, K. W., Hodges, K. V., and Burbank, D. W.: Plio-Quaternary exhumation history of the central Nepalese Himalaya: 2. Thermokinematic and thermochronometer age prediction model. Tectonics, 26(3), 2007.

Whipp, D. M., Ehlers, T. A., Braun, J., and Spath, C. D.: Effects of exhumation kinematics and topographic evolution on detrital thermochronometer data, J. Geophys. Res. Earth Surf., 114, F04021, https://doi.org/10.1029/2008jf001195, 2009.

https://doi.org/10.5194/egusphere-2026-2508
Preprint. Discussion started: 22 May 2026

Whipple, K. X.: The influence of climate on the tectonic evolution of mountain belts. Nature geoscience, 2(2), 97-104, 2009.

Wolff, R., Hetzel, R., Dunkl, I., and Anczkiewicz, A. A.: New constraints on the exhumation history of the western Tauern Window (European Alps) from thermochronology, thermokinematic modeling, and topographic analysis. International Journal of Earth Sciences, 110(8), 2955-2977, https://doi.org/10.1007/s00531-021-02094-w, 2021.